MBoC | ARTICLE

Phospholipase D1 produces phosphatidic acid at sites of secretory vesicle docking and fusion

Broderick L. Bills[a,b], Megan L. Hulser[a,b], and Michelle K. Knowles[a,b,*]
[a]Department of Chemistry and Biochemistry, and [b]Molecular and Cellular Biophysics Program, University of Denver, Denver, CO 80210

ABSTRACT **Phospholipase D1 (PLD1) activity is essential for the stimulated exocytosis of secretory vesicles where it acts as a lipid-modifying enzyme to produces phosphatidic acid (PA). PLD1 localizes to the plasma membrane and secretory vesicles, and PLD1 inhibition or knockdowns reduce the rate of fusion. However, temporal data resolving when and where PLD1 and PA are required during exocytosis is lacking. In this work, PLD1 and production of PA are measured during the trafficking, docking, and fusion of secretory vesicles in PC12 cells. Using fluorescently tagged PLD1 and a PA-binding protein, cells were imaged using TIRF microscopy to monitor the presence of PLD1 and the formation of PA throughout the stages of exocytosis. Single docking and fusion events were imaged to measure the recruitment of PLD1 and the formation of PA. PLD1 is present on mobile, docking, and fusing vesicles and also colocalizes with Syx1a clusters. Treatment of cells with PLD inhibitors significantly reduces fusion, but not PLD1 localization to secretory vesicles. Inhibitors also alter the formation of PA; when PLD1 is active, PA slowly accumulates on docked vesicles. During fusion, PA is reduced in cells treated with PLD1 inhibitors, indicating that PLD1 produces PA during exocytosis.**

SIGNIFICANCE STATEMENT

- Phosphatidic acid (PA) production by Phospholipase D1 (PLD1) activity enhances the stimulated exocytosis of secretory vesicles.
- To determine when and where PLD1 is needed, single docking and fusion events were measured in time.
- PA accumulates at docked vesicles and is formed via PLD1 during fusion.

Monitoring Editor
Avital Rodal
Brandeis University

Received: May 26, 2023
Revised: Nov 29, 2023
Accepted: Dec 13, 2023

This article was published online ahead of print in MBoC in Press (http://www.molbiolcell.org/cgi/doi/10.1091/mbc.E23-05-0189) on December 20, 2023.

AUTHOR CONTRIBUTIONS: B.B. and M.K. conceived and designed the experiments; B.B. and M.H. performed the experiments; B.B., M.H., and M.K. analyzed the data; B.B. and M.K. drafted the article; B.B. and M.K. prepared the digital images.

Conflict of interest: The authors declare no financial conflict of interest.

*Address correspondence to: Michelle K. Knowles (michelle.knowles@du.edu).

Abbreviations used: NPY, neuropeptide Y; PA, phosphatidic acid; PABD, PA binding domain; PLD, phospholipase D; VAMP2, vesicle associated membrane protein 2

INTRODUCTION

Regulated exocytosis is a tightly controlled process in neuroendocrine cells that is essential for the secretion of hormones and neurotransmitters. During exocytosis, the membrane of a docked vesicle fuses with the plasma membrane, a process with a high energy barrier. SNARE proteins have been shown to provide the minimal machinery for fusion (Weber *et al*., 1998) and a few copies, along with their accessory proteins, can provide the energy required (Mohrmann *et al*., 2010; Stepien and Rizo, 2021). While SNARE proteins are vital for exocytosis, lipid rearrangement has been proposed to assist by recruiting protein clusters (Lang *et al*., 2001), recruiting vesicles (Honigmann *et al*., 2013), or stabilizing the highly curved fusion pore (Chernomordik and Kozlov, 2005; Rohrbough and Broadie, 2005;

McMahon *et al.*, 2010). For example, phosphatidylinositol (4,5)-bisphosphate (PI (4,5)P_2) has been shown to inhibit fusion pore dilation (Omar-Hmeadi *et al.*, 2023) and cholesterol is involved with the clustering of Syntaxin1a, a plasma membrane associated SNARE protein essential to docking and fusion (Lang *et al.*, 2001). Lipid-modifying enzymes, such as phospholipase D1 (PLD1), have been implicated as essential in exocytosis (Humeau *et al.*, 2001; Vitale *et al.*, 2001; Hughes *et al.*, 2004; Jenkins and Frohman, 2005; Zeniou-Meyer *et al.*, 2007) and its product, phosphatidic acid (PA), can stabilize negatively curved membranes (Kooijman *et al.*, 2003; Chernomordik and Kozlov, 2005; Callan-Jones *et al.*, 2011; Bills and Knowles, 2022).

There are six PLD isoforms in mammals, with PLD1 and PLD2 acting as lipases positioned within to play a role in exocytosis (Brown *et al.*, 1998; Vitale *et al.*, 2001; Cockcroft *et al.*, 2002; Hughes *et al.*, 2004; Jenkins and Frohman, 2005). PLD1 and PLD2 use the substrate phosphatidylcholine to produce PA (Frohman, 2015). PLD1 and PLD2 primarily differ in basal activity; PLD2 is constitutively active and PLD1 is stimulated (Peng and Frohman, 2012). Several studies have shown that inhibition and knockdowns of PLDs reduce exocytosis (Humeau *et al.*, 2001; Vitale *et al.*, 2001; Hughes *et al.*, 2004; Jenkins and Frohman, 2005; Zeniou-Meyer *et al.*, 2007). Specifically, PLD1 is essential for exocytosis in platelets, HL-60 cells, PC12 cells, and chromaffin cells (Haslam and Coorssen, 1993; Stutchfield and Cockcroft, 1993; Zeniou-Meyer *et al.*, 2007, 2009), where the loss or inhibition of PLD1 diminishes secretion, demonstrating that that PLD1 or PA is required. However, PLD2 has also been shown to be involved in exocytosis, particularly in mast cells, where PLD1 and PLD2 are involved at different stages (Choi *et al.*, 2002). Overall, PLD1 is required for stimulated exocytosis in most secretory cells, and it is likely that the formation of PA is essential.

PLD1 localizes partially to the plasma membrane (Brown *et al.*, 1998; Freyberg *et al.*, 2001; Hozumi *et al.*, 2022), and its activity increases during stimulation leading to the formation of PA at the plasma membrane (Zeniou-Meyer *et al.*, 2007; Tanguy *et al.*, 2020). PA formation has typically been observed by the recruitment of the PA-binding domain (PABD) of Spo20 to the plasma membrane (Zeniou-Meyer *et al.*, 2007, 2009; Tanguy *et al.*, 2022). However, new dyes have been designed to show where PA is newly formed, using click chemistry and relying on PLD activity (Bumpus and Baskin, 2017). One hypothesis for the role of PA is during the membrane fusion step of secretion, where PA could stabilize the highly curved fusion pore (Kooijman *et al.*, 2003; Chernomordik and Kozlov, 2005; Callan-Jones *et al.*, 2011; Bills and Knowles, 2022). PA is an inverse conical lipid containing a small, negatively charged headgroup with two fatty acid tails. PA has been established as preferring negative curvature in in vitro studies (Kooijman *et al.*, 2003, 2005; Bills and Knowles, 2022). However, precisely when and where PA is formed during exocytosis is currently lacking.

To test whether PLD1 is present at fusing vesicles and determine when and where the production of PA is required, a model secretory cell line (PC12) was used to express either GFP-PLD1 or GFP-PASS, a PA biosensor similar to PABD (Zhang *et al.*, 2014). Cells were imaged using total internal reflection fluorescence (TIRF) microscopy and the presence of PLD1 and the formation of PA were compared with the location of secretory proteins: Syntaxin-1a (Syx1), vesicle-associated membrane protein 2 (VAMP2) and neuropeptide Y (NPY). Single fusion events were imaged at high speed to measure the recruitment of PLD1 and the formation of PA as vesicles docked and fused with the plasma membrane. Colocalization analyses under basal, stimulated, and inhibitory conditions demonstrate that PLD1 is present on docked, fusing, and moving vesicles and colocalizes with Syx1 clusters. The presence of PLD1, however, does not solely determine where PA is produced. Although PLD1 is present on vesicles, the production of PA only occurs after vesicles dock and after membrane fusion. The production of PA at these stages requires PLD1.

RESULTS

PLD1 localizes to secretory vesicles and Syx1 clusters

To determine the role of PLD1 in secretory vesicle secretion, PC12 cells were transiently transfected with GFP-PLD1 and either VAMP2-pHmScarlet, NPY-mCherry or Syx1-mCherry. GFP-PLD1 visually colocalizes to all three proteins (Figure 1, A-C). To measure the extent of

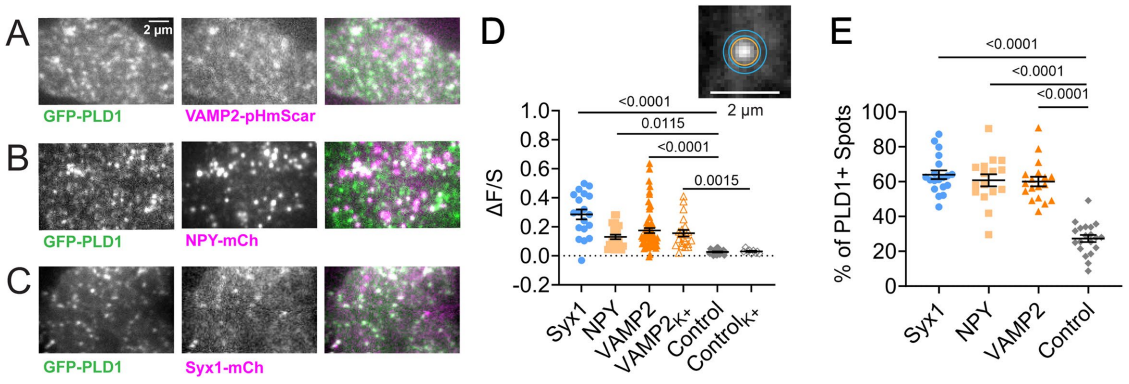

FIGURE 1. Phospholipase D1 colocalizes with secretory vesicle markers and syntaxin clusters. (A–C) PC12 cells were transfected with GFP-PLD1 (left) and (A) VAMP2-pHmScarlet, (B) NPY-mCherry, or (C) Syx1-mCherry (middle) and imaged at room temperature using TIRF microscopy. The overlays (right) are white where colocalization occurs. Scale bar: 2 µm. (D) The extent of GFP-PLD1 accumulation, ΔF/S, at Syx1 clusters (blue circles), NPY spots (light orange squares), or VAMP2 spots (dark orange triangles). As a control, ΔF/S was measured for cytosolic GFP at VAMP2 spots (gray diamonds). Empty symbols represent ΔF/S of PLD1 or cytosolic GFP in cells stimulated with 60 mM KCl. Lines and errors are mean and SEM. Black bars and numbers above represent *p*- values between PLD1 at sites of the indicated protein compared with cytosolic GFP at VAMP2+ vesicles. Each spot represents one cell. At least 10 cells from at least three independent experiments were conducted for each condition. *Inset*: description of ΔF/S measurements, where $\frac{\Delta F}{S} = \frac{C-A}{A-bg}$. The circle, C, Is represented by the orange circle, while annulus A is the space between the cyan circles and bg is the average intensity surrounding the cell. (E) The JACoP plugin in ImageJ was used to identify the percentage of Syx1a or vesicle locations with PLD1 or cytosolic GFP. All statistics are described in the Materials and Methods.

colocalization, an object-based analysis was used where locations of interest, such as Syx1a clusters and secretory vesicles, were located and the GFP-PLD1 intensity was measured at these sites. To quantify the amount of GFP-PLD1 at sites of interest, the intensity within a circle centered around the vesicle or Syx1 cluster location was measured relative to the local background (ΔF = circle – annulus, shown in Figure 1D). This was normalized by the expression level (S = annulus – background outside of the cell). A positive value indicates that GFP-PLD1 is present at VAMP2-containing vesicles, NPY vesicles, or Syx1 clusters. GFP-PLD1 significantly localizes to all three compared with a negative control: cytosolic GFP. Upon stimulation with high K^+ buffer, Ca^{2+} enters PC12 cells and fluorescence from a calcium indicator increases (Supplemental Figure S1). All cells were labeled with CellMask (Supplemental Figure S1A) and Fluo4-AM (Supplemental Figure S1, B and C). The only cells that did not show a change indicating the influx of Ca^{2+} were cells that were part of a larger cluster of cells (Supplemental Figure S1, D and E); therefore, single cells or pairs of cells were measured for the remaining experiments. No increase in colocalization was observed for PLD1 at VAMP2 positions after 2 min of stimulation (Figure 1D). To further confirm PLD1 localization, the JACoP plugin in ImageJ was used to identify the percentage of PLD1+ vesicles and Syx clusters, which are all significantly higher than cytosolic GFP at VAMP2 vesicles (Figure 1E). Additionally, to verify that green bleed through into the red channel was not causing the observed colocalization, zoomed in locations of cells expressing GFP-PLD1 and a red marker were examined. Many green spots do not show a red spot in the same position (Supplemental Figure S1F). Overall, PLD1 is positioned to play a role in is exocytosis, in line with what others have shown (Brown *et al.*, 1998; Vitale *et al.*, 2001; Cockcroft *et al.*, 2002; Hughes *et al.*, 2004), and stimulation does not alter the position of PLD1 over a short period of time.

One limitation of using GFP-PLD1 is that some studies suggest that overexpression of PLD1 leads to mislocalization (Freyberg *et al.*, 2001). By eye, GFP-PLD1 is extremely low expressing as noted by how dim cells were on the microscope, suggesting that transient expression in PC12 cells is low. To quantify the amount of overexpression a slot blot of PLD1 from transiently transfected cells was compared with endogenous PLD1 expression (Supplemental Figure S2A). PLD1 is increased by 4.3% in a Western blot of all cells (transfected and nontransfected), where about 25% of cells are transfected (Supplemental Figure S2), therefore it is overexpressed by approximately 17% in transfected cells. Additionally, a different PLD1 construct with an internal GFP label has been created with the goal of moving the GFP moiety away from membrane-binding motifs (Corrotte *et al.*, 2006.). To determine whether the colocalization that was observed with GFP-PLD1 (Figure 1) was also present with endogenous PLD1, immunofluorescence was performed on fixed cells; anti-PLD1 is present at sites of VAMP2-pHluorin (Supplemental Figure S2D). This suggests that the N-terminal GFP tag and overexpression is not altering the position of PLD1 in PC12 cells.

GFP-PLD1 is present on mobile VAMP2 vesicles and during docking, fusion

To assess whether PLD1 is recruited as vesicles traffic to the plasma membrane, dock, and then fuse, cells expressing GFP-PLD1 and VAMP2-pHmScarlet were imaged in time using TIRF microscopy. VAMP2-pHmScarlet is visible prior to fusion and also increases in fluorescence due to the large pH change that occurs upon fusion (Liu *et al.*, 2021), making it an excellent probe for visualizing moving, docking, and fusing vesicles in a single-color channel. VAMP2-pHmScarlet vesicles were located using a previously established method (Mahmood *et al.*, 2023), then divided into three classes: visiting, docking, or fusing vesicles based on whether they move through a cropped movie (Figure 2A), appear and remain static (Figure 2B), or appear, increase quickly in intensity and spread out from the center (Figure 2C). To quantify the data, the intensity within a circular region (Figure 1D, inset orange) was measured in time and the average of five frames prior to the event onset (–0.5 to –0.1 s) was subtracted and normalized (see *Materials and Methods*). Note that the annulus was not used in this measurement because it changes in intensity when fusion occurs as fluorescence radially expands. The whole trace was then normalized by the maximum intensity. To visualize this change, events were averaged into one movie and then 5-frames at fusion and visitor onset (–0.5 to –0.1 s, "initial") and VAMP2 peaks or plateaus ("final") were averaged (Figure 2, D–F, top row). To highlight the change that occurs in the GFP-PLD1 intensity during the events, the initial image was subtracted from the final image to create a difference image ("Δ"). All GFP-PLD1 difference images show spots in the center. As a control, cytosolic GFP was expressed in place of GFP-PLD1 (Figure 2, D–F, bottom row). The intensity in time is shown for both the vesicle (Figure 2, G–I, purple) and PLD1 (Figure 2, G–I, green) such that 0 s is the beginning of the rise in VAMP2 intensity and the onset of the vesicle fusion, docking or visiting. In all three types of events, the intensity of GFP-PLD1 significantly increases after the onset of visiting, docking, or fusion (Figure 2, D–I), suggesting that PLD1 is carried on VAMP2 vesicles. Interestingly, during fusion (Figure 2I), the loss of PLD1 occurs faster than the loss of VAMP2 from the fusion site, possibly due to different rates of diffusion on the membrane. In all types of events, cytosolic GFP was used as a control and an increase in intensity is not observed (Figure 2, G–I; Supplemental Figure S3). This suggests that PLD1 is present on moving VAMP2 vesicles and more may be recruited during docking and fusion.

Inhibition of PLD1 reduces the fusion of VAMP2 vesicles and vesicle mobility but does not alter PLD1 localization

One key feature of PLD1 is its ability to convert PC into PA, where the lipid PA is then involved trafficking (Brito de Souza *et al.*, 2014; Luo *et al.*, 2017; Tanguy *et al.*, 2022) and fusion (Humeau *et al.*, 2001; Vitale *et al.*, 2001; Hughes *et al.*, 2004; Jenkins and Frohman, 2005; Zeniou-Meyer *et al.*, 2007). To explore the activity of PLD1, PC12 cells expressing GFP-PLD1 and VAMP2-pHmScarlet were transfected with control or PLD1 siRNA. Fusion rates were reduced by ~70% under knockdown conditions, which was not rescued by transfecting cells with GFP-PLD1 (Figure 3A). This rescue possibly failed due to the very low expression of GFP-PLD1 in PC12 cells (Supplemental Figure S2). Further testing was conducted with PLD inhibitors, either 100 nM FIPI, a pan-PLD inhibitor or 500 nM VU0155069, a PLD1-specific inhibitor. To verify whether fusion is blocked in the presence of inhibitors, the rate of fusion was measured. The frequency of fusion was significantly reduced in K^+-stimulated cells when cells were treated with siRNA (Figure 3A). PLD1 and PLD1/2 inhibitors (Figure 3B) reduced fusion to a similar extent, however, the localization of GFP-PLD1 to sites of fusion was not significantly affected (Figure 3C). The inhibition of PLDs also altered the rate vesicles near the plasma membrane moved. VAMP2 vesicles were tracked in time and the rate of motion was measured. Diffusion coefficients of VAMP2+ vesicles in cells treated with inhibitors were slightly slower (Supplemental Figure S4A). However, when only mobile vesicles ($D > 0.0055\ \mu m^2/s$) were counted (Supplemental Figure S4B), the reduction in motion vanishes, suggesting that the reduction observed is due to a change in the number of mobile vesicles. Interestingly, the fraction of mobile vesicles per cell

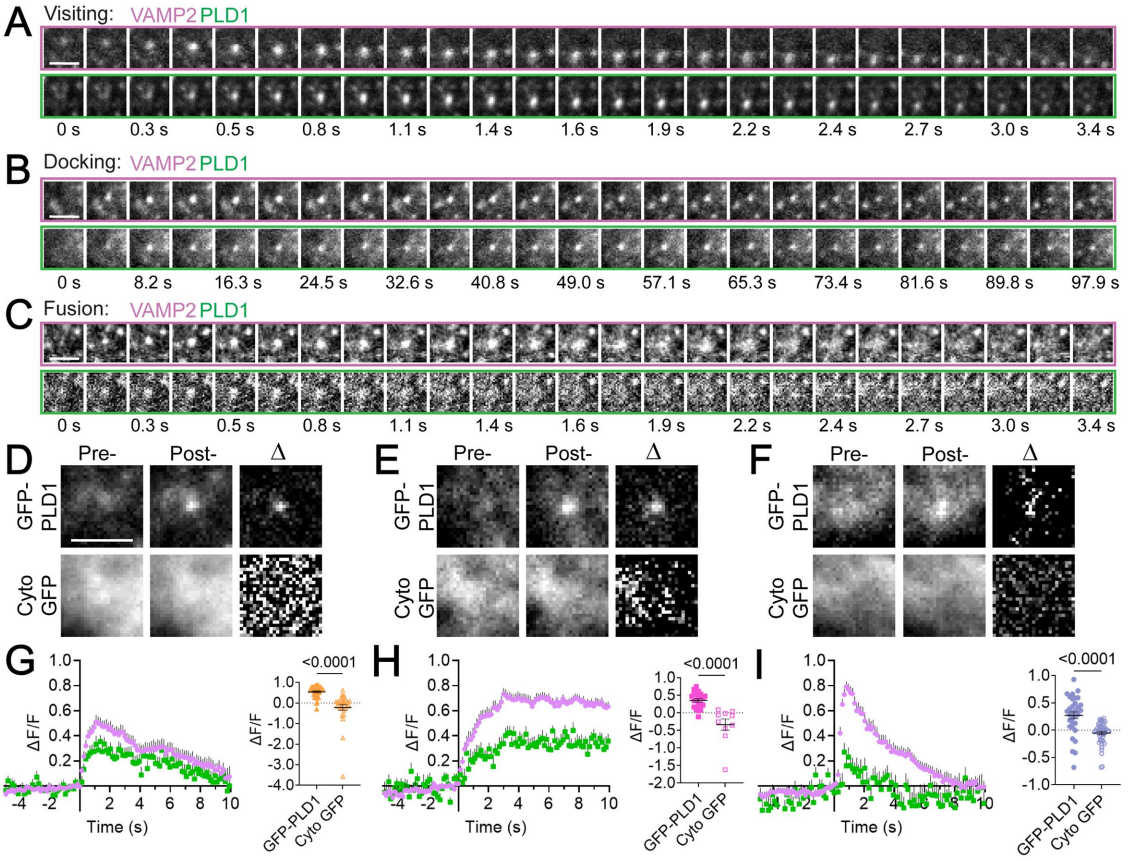

FIGURE 2. GFP-PLD1 localizes to visiting, docking, and fusing VAMP2 Vesicles. PC12 cells expressing GFP-PLD1 and VAMP2-pHmScarlet were imaged at 136 ms/frame at room temperature. (A–C) Single vesicle events were located using an automated algorithm that identifies three types of events: visiting (A), docking (B), or fusing (C) vesicles. Top rows: montages of VAMP2-pHmScarlet. Bottom rows: corresponding montages of GFP-PLD1, where each image is a 5-frame average. Scale bars: 2 μm. (A–C) are examples of a single event. (D–F) Average images of many events prior to visiting (D, 17 PLD1 and 22 GFP events), docking (E, 18 and 10 events), or fusion (F, 22 and 25 events) at the onset (left) and peak/plateau VAMP2 intensity (middle) for PLD1 (top) or cytosolic GFP (bottom). A difference image, Δ, of each is shown to highlight changes (right). Initial and final images are contrasted the same. Scale bar: 2 μm. (G–I) Left: traces of (G) visiting ($n = 37$), (H) docking ($n = 20$), and (I) fusing ($n = 32$) vesicles for GFP-PLD1 (green) and VAMP2-pHmScarlet (purple). The intensity, ΔF/F, was normalized to 1.0 for each event prior to averaging. Graphs depicting ΔF/F values of GFP-PLD1 (solid symbols) and cytosolic GFP (empty symbols) at the peak of the VAMP2 traces or at 80% of the plateau. Each spot represents one event for cytosolic GFP (7 cells, three replicate experiments) or GFP-PLD1 (17 cells, six replicate experiments). Line and error are mean and SEM; all statistics are described in the *Materials and Methods*.

does not significantly decrease upon treatment with either inhibitor (Supplemental Figure S4C). Therefore, the activity of PLD1 impacts the mobility and fusion of VAMP2+ vesicles but does not contribute to the location of PLD1.

PA accumulates at fusion sites and this depends on PLD1 activity

If PLD1 activity is essential to fusion, the formation of PA should occur and the timing of PA formation during the fusion process can be determined by imaging single fusion events. To test this, fusion events were located in cells expressing VAMP2-pHmScarlet and GFP-PASS analogous to the approach shown for GFP-PLD1 (Figure 2). GFP-PASS is a PA-binding protein tagged to mGFP and marks regions of the cell that are enriched in PA (Zhang *et al.*, 2014). Visiting, docking, and fusion events were identified, and average GFP-PASS images were calculated from events prior to visiting (Figure 4A), docking (Figure 4B) or fusing (Figure 4C) vesicles. Figure 4 shows the PASS accumulation only and PASS does not show up during the initial 2–3 s over which the images are shown for vesicles that move (Figure 4A) or dock (Figure 4B). However, during fusion, GFP-PASS increases quickly (Figure 4C). A difference image visualizes the change in PA via the GFP-PASS intensity in all three classes of events (Figure 4, A-C). To quantify the intensity change, the ΔF/F of PASS during visiting, docking, and fusion were calculated (Figure 4, D–F). Unlike PLD1, PASS does not significantly increase immediately upon visiting or docking but does increase during fusion (Figure 4G), reaching a maximum 1.4 s after the peak of the VAMP2 fusion event (Figure 4H).

PA has been hypothesized to accumulate at negatively curved regions within the fusion pore, which suggests that the amount of PA could possibly affect the release rate of content post-fusion. To probe whether the presence of PA affects the fusion kinetics, the slope of the decay of VAMP2 from the peak fluorescence to 1 s later and the GFP-PASS intensity (ΔF/S) was measured for single fusion events. It is useful to note that the measurement ΔF/S is normalized by the local background (S) and conveys enrichment at the vesicle position, and this is insensitive to the expression level within a range (Barg *et al.*, 2010). The initial ΔF/S of GFP-PASS was plotted against

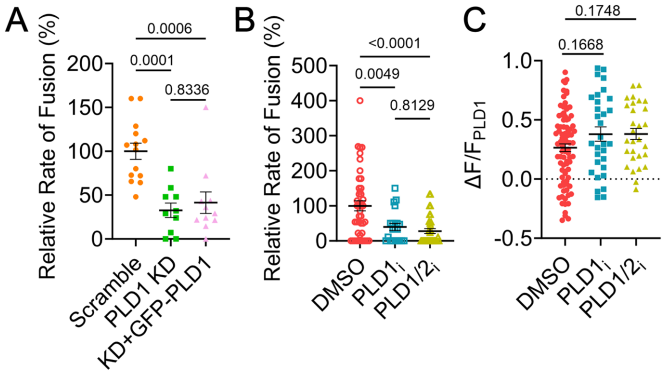

FIGURE 3. PLD knockdown and inhibition reduces fusion rates. (A) PC12 cells were treated with siRNA (scramble, orange circles or PLD1 siRNA, green squares, and pink triangles) and expressed VAMP2-pHmScarlet (orange circles and green squares) or VAMP2-pHmScarlet and GFP-PLD1 (pink triangles). Fusion events were identified and counted in cells stimulated with 60 mM KCl, then divided by the average rate of fusion in Scramble cells to account for day-to-day variation. Each point represents one cell from three independent experiments. (B) PC12 cells expressing VAMP2-pHmScarlet and GFP-PLD1 were treated with inhibitors for PLD1 (VU0155069, 500 nM), PLD1 and 2 (FIPI, 100 nM), or a similar amount of DMSO (control). Cells were incubated 30 min prior to imaging and imaged at 37°C. The relative frequency of VAMP2 fusion events decreases with inhibition. This includes spontaneous and evoked fusion. Each point is one cell from at least four independent experiments. (C) The intensity (ΔF/F) of PLD1 at peak VAMP2 intensity during fusion in DMSO, PLD1i, or PLD1/2i-treated cells. Each point is one fusion event. Lines are mean values, error bars are SEM. All statistics are described in the *Materials and Methods*.

the initial decay of the VAMP2 intensity postfusion (Supplemental Figure S5) and a negative correlation was noted (Pearson's correlation coefficient = -0.1744), which indicates a higher PA presence during faster fusion events. Therefore, the rate of decay was binned into "fast" and "slow" events based on the histogram of slopes (Supplemental Figure S5). There is more GFP-PASS present on faster events (Figure 4I).

To probe whether PA is produced by PLD1 during fusion rather than recruited or produced by other means, PC12 cells expressing GFP-PASS and VAMP2-pHmScarlet were treated with inhibitors for PLD1 or PLD1/2 and compared with a vehicle control, as previously described (Figure 3). Cells were stimulated with K+ during imaging. Due to the fact that PLD inhibitors reduce fusion events (Figure 3, A and B), the number of events observed in cells treated with inhibitors was low. GFP-PASS intensity from fusion locations were averaged before and during fusion, and the difference between the two was measured (Figure 5, A-C, *inset*). The average fusion traces were plotted (Figure 5, A–C, purple) alongside the GFP-PASS intensity (Figure 5, A–C, blue). To quantify whether PLD1 inhibition altered the recruitment of GFP-PASS during fusion, the change in GFP-PASS intensity was measured at the time that coincided with the peak of the VAMP2-pHmScarlet intensity relative to the prefusion intensity (Figure 5D). All inhibitory conditions show a decrease in PASS intensity, possibly due to new membrane lacking GFP-PASS being added to the fusion site. However, GFP-PASS increases in intensity in control conditions and this is significantly more than when PLD is inhibited (Figure 5D). Because these inhibitors do not affect other PA-producing enzymes, like diacylglycerol kinase, this reduction of GFP-PASS intensity is likely due to PLD1 and the lack of PA.

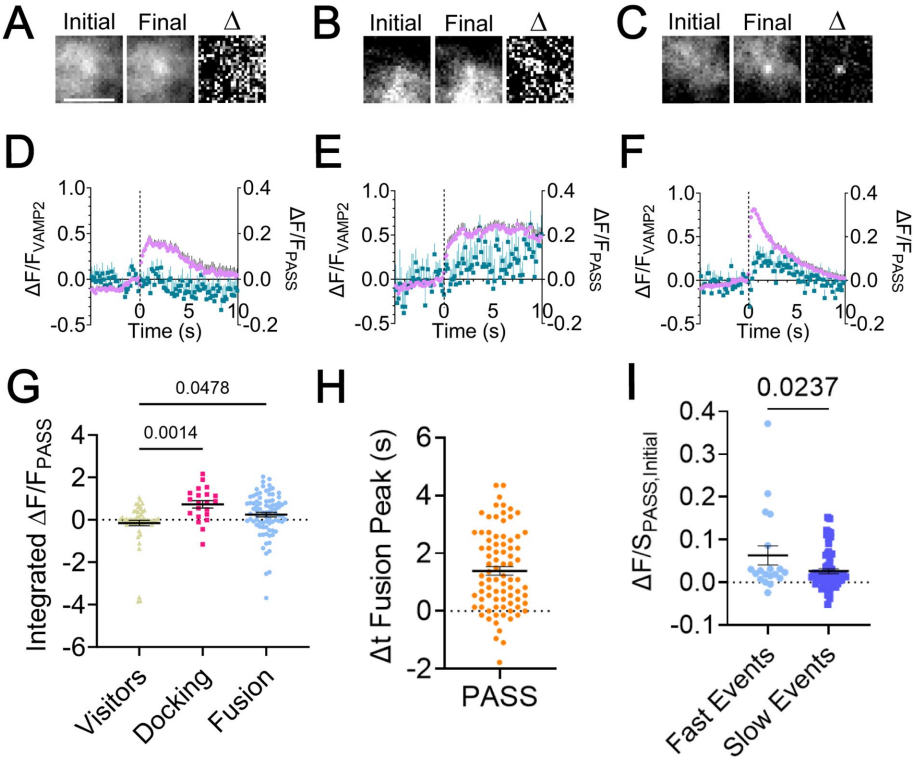

FIGURE 4. PA is present during fusion and docking. PC12 cells were transfected with GFP-PASS, a PA-binding protein, and VAMP2-pHmScarlet, then cells were imaged to visualize (A) visiting, (B) docking, and (C) fusing vesicles. (A–C) Average images of GFP-PASS prior to onset (left), at the peak (middle) of the VAMP2 intensity, and a difference image between the two (right). Scale bar: 2 μm. Before and after images are contrasted identically and are averages of 5 frames (n = 51, 12 and 46 for [A–C], respectively). (D–F) Average intensity (ΔF/F) traces of VAMP2-pHmScarlet (purple circles) and GFP-PASS (teal squares). Error bars are SEM (n = 62, 21, 83 events for D–F, respectively, from at least 8 cells and three independent experiments). (G) Integrated intensity of GFP-PASS from 0 to 4 s after the fluorescence onset of VAMP2 during visiting, docking, or fusing events. Each point represents one event from three independent experiments. (H) Time from peak VAMP2 intensity to peak PASS intensity. Each point represents one event. (I) Initial VAMP2 decay slopes were binned into fast and slow events and the amount of PASS present was measured for each. Fast events have more PASS present. (G–I) Lines are mean values, error bars are SEM; all statistics are described in the *Materials and Methods*.

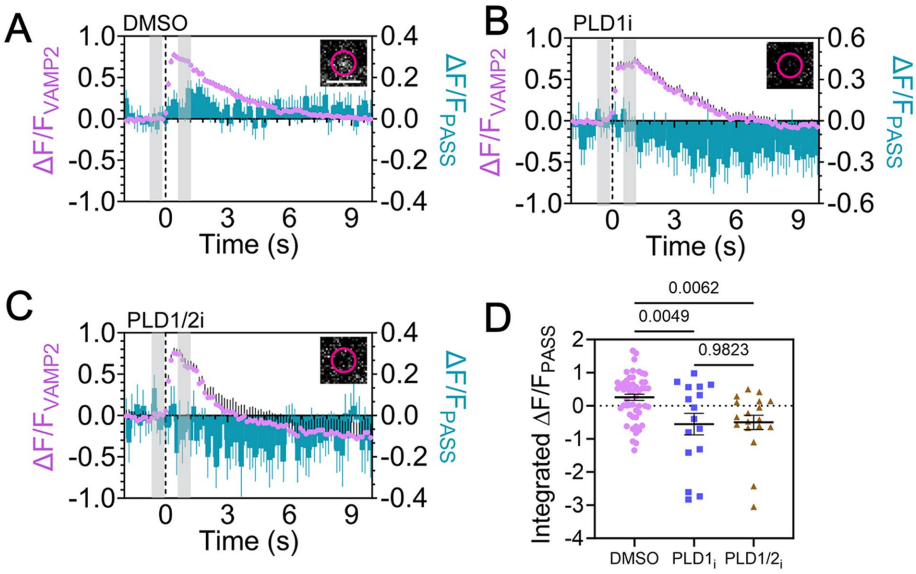

FIGURE 5. Inhibition of PLD1 reduces the amount of PA present during fusion. PC12 cells were transfected with GFP-PASS (a PA marker) and VAMP2-pHmScarlet, then cells were imaged at 37°C to visualize fusing vesicles in the presence of PLD inhibitors. (A) Control cells treated with DMSO ($n = 40$ cells, 52 fusion events). (B) Cells treated with PLD1-specific inhibitor ($n = 12$, 16 fusion events). (C) Cells treated with a pan-PLD inhibitor ($n = 13$, 19 fusion events). *Inset:* Average image showing the change in PASS intensity, where the average image from five frames immediately prior to fusion was subtracted from the average PASS image (5 frames) that coincides with the VAMP2 peak. The time regions are shown in the gray rectangles and the scale bar is 2 μm. In (A–C) the average normalized intensity traces of fusion events is shown for VAMP2-pHmScarlet (purple) and GFP-PASS (cyan). (D) Integrated PASS intensity from 0 to 4 s after the onset of the VAMP2-pHmScarlet fusion event. Lines are mean values, error bars are SEM; all statistics are described in the *Materials and Methods*.

PA accumulates at vesicle locations after docking and throughout exocytosis

PA is present near vesicle docking sites in EM data (Zeniou-Meyer *et al.*, 2007) and accumulates on the plasma membrane minutes after stimulation (Tanguy *et al.*, 2020). To determine the time course of PA arrival after vesicles dock, cells were stimulated with high K^+ and GFP-PASS was imaged and quantified during docking for 10 seconds after the initial docking event (Figure 6, A and B). Difference images show the increase of PASS at the docking cite (Figure 6A, bottom). After 10 s, the GFP-PASS signal is significantly larger than the cytosolic-GFP control (Figure 6C), and the GFP-PASS signal gradually increases as time goes on (Figure 6B). To identify whether PA is formed or accumulated during vesicle docking, PLD inhibitors were used and both inhibitors block the formation of PA (Figure 6D), therefore PA is formed by PLD1 during docking events and PLD2 cannot compensate for PLD1 inhibition. When the intensity of GFP-PASS is measured relative to the amount present prior to docking (considered a nonspecific, background fluorescence because GFP-PASS is present in the cytoplasm), the intensity of GFP-PASS increases slowly after docking, then more prior to fusion, reaching a maximum postfusion (Figure 6E). If cytosolic GFP is expressed in place of GFP-PASS, this intensity increase is not observed (Supplemental Figure S6). Therefore, PA formation increases throughout the entire exocytosis process, from moving to docking to fusion, as exocytosis progresses. This places PA in a position to regulate several stages of membrane fusion.

DISCUSSION

In this work, we demonstrate that the production of PA via PLD1 activity impacts exocytosis in PC12 cells. The inhibition of PLD1 or PLD1 and 2 reduces fusion events (Figure 3, A and B). Specifically, PLD1 is required for fusion and the presence of PLD2 cannot compensate for the inhibition of PLD1 in PC12 cells (Figure 3). This agrees with the work of others, where the loss of PLD1 function by inhibitors, siRNA, or KO reduces stimulated secretion (Tanguy *et al.*, 2022) and the frequency of fusion events in chromaffin cells (Tanguy *et al.*, 2020). A wide variety of cells, such as adipocytes (Huang *et al.*, 2005), endothelial cells (Disse *et al.*, 2009), mast cells (Choi *et al.*, 2002), and neuroendocrine cells (Zeniou-Meyer *et al.*, 2007, 2009), need PLD1 for proper secretion, albeit some cell types (mast cells) also use PLD2 during different stages of exocytosis (Choi *et al.*, 2002).

By imaging single secretory vesicles concurrent with PLD1, PLD1 can be shown to localize with secretory vesicles, as well as Syx1 clusters under basal conditions, suggesting an association between PLD1 and secretory machinery (Figure 1). This places PLD1 in a position to act when needed. As single vesicles were observed to visit the plasma membrane or dock, PLD1 intensity significantly increased (Figure 2, A, B, D, E, G, and H), indicating that PLD1 is trafficked on secretory vesicles. In regard to docking and visiting vesicles, the PLD1 intensity increase could be attributed to an increase in excitation as the vesicle moves into the TIRF field or an increase in the amount of PLD1, and these conclusions are challenging to disentangle. Therefore, we conclude that PLD1 is on vesicles as they dock and move near the plasma membrane and these results align with the established role of PLD1 in trafficking (Brito de Souza *et al.*, 2014; Luo *et al.*, 2017; Tanguy *et al.*, 2022) and exocytosis (Humeau *et al.*, 2001; Vitale *et al.*, 2001; Hughes *et al.*, 2004; Jenkins and Frohman, 2005; Zeniou-Meyer *et al.*, 2007).

One main function of PLD1 is to catalyze the production of PA from PC, where the formation of PA has been shown to interact with the polybasic region of Syx1a clusters (Lam *et al.*, 2008) and hypothesized to stabilize negative curvature within the fusion pore (Zeniou-Meyer *et al.*, 2007; Gasman and Vitale, 2017). The role of PA and positioning of PLD1 is depicted in Figure 7 for docking, fusing, and visiting vesicles. Through high spatial and temporal imaging of single vesicles, the formation of PA was observed after vesicles stably dock (Figure 6, A–C) and this formation requires PLD1 (Figure 6D). PASS is not present on vesicles that merely visit the plasma membrane (Figure 4, A–D) and the GFP-PASS intensity does not immediately increase as vesicles dock (Figures 4, B–E), suggesting that PA is not carried on vesicles. However, the rate that PASS binds to PA is a factor that needs to further examined to better understand the timing of PA formation. Others have noted that PA is enriched on vesicles (Kassas *et al.*, 2017). It is possible that PA is on the inner leaflet or PASS is restricted from vesicular PA, like others have noted

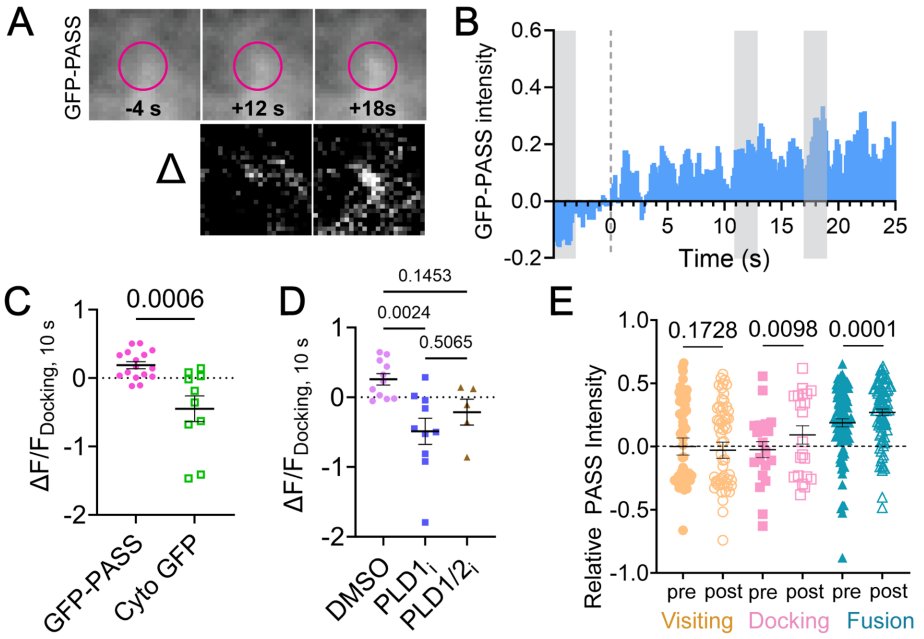

FIGURE 6. PLD1 produces PA at docked vesicles over time in stimulated cells. (A) Average images ($n = 13$ events) of PASS before onset of docking (−4 s), after 8 s, and after 12 s postdocking (top). Pink circles mark the location of the docked vesicle. The difference between pre- and postdocking images (bottom). Initial and final images are contrasted identically. (B) The average ΔF/F trace of GFP-PASS over extended periods of time after stimulation with 60 mM KCl. The gray boxes refer to the times shown in (A). (C) ΔF/F of PASS (pink circles) and GFP (green squares) 10 s after docking. One dot corresponds to one docking event. (D) ΔF/F of PASS 10 s after docking in cells treated with DMSO (purple circles) with or without PLD1 inhibition (blue squares) or PLD1/2 inhibition (brown triangles). (E) The relative PASS intensity was measured over the different stages of membrane fusion: visiting (orange), docking (pink), and fusion (blue). The PASS preintensity (visiting) was subtracted from all to obtain a relative intensity. The "pre" intensity was measured at 0.5 to 0.1 s prior to the event. The post-docking intensity (pink, open squares) was measured after several seconds, when single events reached the plateau intensity in the VAMP2-pHmScarlet channel. The postfusion intensity (blue, open triangles) was measured when the VAMP2-pHmScarlet intensity was at a maximum. Lines in (C–E) are mean values, error bars are SEM. All statistics are described in the *Materials and Methods*.

with the related probe, PABD of Spo20 (Carmon *et al.*, 2020). Vesicles dock and PA slowly accumulates (Figure 6, A–C). It is not clear, in our work, whether PA formation occurs on the vesicle membrane or the plasma membrane, but ultrastructural studies show the accumulation of PA near or on the plasma membrane near docked vesicles (Zeniou-Meyer *et al.*, 2007). PA accumulation at the plasma membrane poststimulation has also been observed in PC12 cells using cellular fractionation and mass spectrometry methods (Zeniou-Meyer *et al.*, 2007; Tanguy *et al.*, 2020) and an increase in PA at the plasma membrane was also observed using fluorescence microscopy (Zeniou-Meyer *et al.*, 2007). Together, this suggests that PA forms on the plasma membrane after docking. Similar to other fusion regulatory molecules, PA is not present in a cluster prior to docking; Syx1a clusters form after vesicles approach the membrane and Syx1a clusters are required for stable docking (Barg *et al.*, 2010; Knowles *et al.*, 2010). PA also accumulates after vesicles dock, and we hypothesize that PA could be retained at the docking site via the established interaction with Syx1a (Lam *et al.*, 2008).

We initially expected an increase in immobile/docked vesicles upon PLD knockdowns or inhibition because fusion was inhibited (Figure 3, A and B), therefore vesicles should be waiting at the membrane, unable to secrete. However, the number of immobile vesicles was not significantly different with inhibition (Supplemental Figure S4A). This supports the idea that PA production at docking sites aids in stabilizing the protein machinery necessary for docking. This could occur through proteins that are known to aid in docking and interacting with PA, such as Syx1a. Syx1a clusters are stabilized by PA (Lam *et al.*, 2008), essential for docking in neuroendocrine cells (Knowles *et al.*, 2010), and PLD1 accumulates at Syx1a clusters (Figure 1D). Others have noted that a longer treatment of high K^+ during PLD inhibition reduced docked vesicles in EM data (Tanguy *et al.*, 2020), further supporting the model that PA forms due to PLD activity at vesicle docking sites. Overall, our findings suggest PA formation could be a hallmark of docked vesicles, possibly acting through Syx1a.

After secretory vesicles initially dock, the amount of PA at docked vesicle positions gradually increases (Figure 6B) and continues to increase throughout the stages of exocytosis where PA is present immediately prior to fusion (Figure 6E). PA then increases postfusion (Figures 4, C and F and 6E) where GFP-PASS intensity hits a maximum at 1.4 s postfusion, on average (Figure 4H). To determine the source of PA, PLD1 and PLD1 and 2 were inhibited (Figure 5). Both inhibitors stop the accumulation of PASS at fusion sites, demonstrating that PLD1 is responsible for PA that accumulates postfusion and the presence of PLD2 cannot compensate. PA could form in situ at the vesicle location or be recruited from PLD1 formed PA that is already present on the plasma membrane. Both potential sources of PA require PLD1 and cannot be compensated with PLD2 (Figure 5).

It is interesting to note that PLD1 is present in places where PA is not observed. For example, PLD1 is on both moving and docking vesicles (Figure 2), yet PA forms postdocking and postfusion. This suggests that PLD1 is waiting for activation to begin PA production. PLD is activated by the V-ATP synthase subunit V0a1 and this interaction requires ARNO, a GEF protein for Arf6, which is an established PLD regulator (Galas *et al.*, 1997; Caumont *et al.*, 1998, 2000; Yang and Mueckler, 1999; Vitale *et al.*, 2002a, 2002b; Matsukawa *et al.*, 2003; Liu *et al.*, 2005; Béglé *et al.*, 2009; Pelletán *et al.*, 2015; Wang *et al.*, 2023). This interaction happens after stimulation, suggesting that Ca^{2+} entry starts a cascade of events that leads to PA production, through these regulatory proteins. Therefore, PLD1 is present in positions where PA production could be needed, but only produces PA after activation.

Because PA is observed to be present postfusion and PA is hypothesized as a lipid that stabilizes the fusion pore, we were curious whether the amount of PA correlated to the rate of release as measured by the loss of VAMP2 from the fusion site. After binning fast fusion events from slow fusion events, more PA was observed at fast events (Figure 4I; Supplemental Figure S5). The role of PA in membrane fusion is likely coupled to the proteins it interacts with. In the case of PI (4,5)P_2, more PI (4,5)P_2 slowed fusion by recruiting endocytic proteins that restrict fusion pore expansion

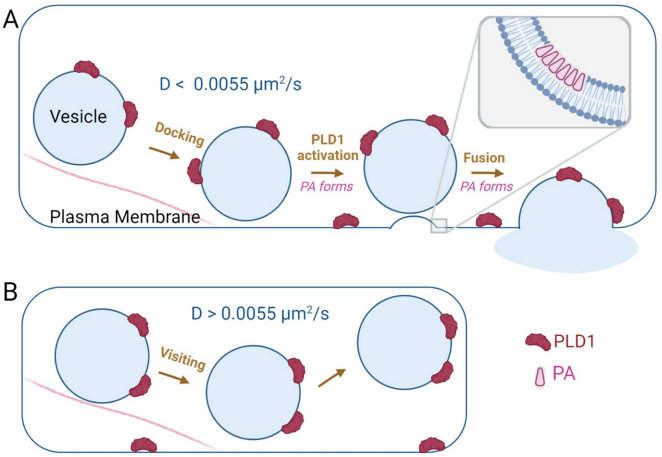

FIGURE 7. Model of PLD1 activity and localization. (A) During docking and fusion, PA forms postdocking over the course of 10 seconds and postfusion, within seconds. *Inset:* A zoomed in look at the hypothesized role of PA prefusion at the gray box shown. PA has been shown to induce or sort at regions of negative membrane curvature and is hypothesized to assist with the membrane shape changes during fusion. (B) Visiting secretory vesicles carry PLD1 but PA is not produced during movement. Moving vesicles move at a diffusion rate of 0.0055 μm²/s or higher. Figure created with BioRender.com.

(Omar-Hmeadi *et al.*, 2023). Similarly, PA could also act by interacting with proteins that assist with fusion and future studies could assess the proteins involved.

Overall, PLD1 has been established as necessary for stimulated exocytosis (Humeau *et al.*, 2001; Vitale *et al.*, 2001; Hughes *et al.*, 2004; Jenkins and Frohman, 2005; Zeniou-Meyer *et al.*, 2007). The results shown in this work support the hypothesis that PLD1 is involved due to its production of PA. PLD1 is present on vesicles, and PA is formed after vesicles dock and PA accumulates at the fusion site postfusion. In both cases, the formation of PA depends on PLD1 activity, which cannot be compensated by PLD2.

MATERIALS AND METHODS

Request a protocol through *Bio-protocol*.

Cell culture

PC12-GR5 cells (gift from Dr. Wolf Almers) were cultured in flasks in Dulbecco's modified eagle medium (DMEM, Thermo Fisher Scientific, Waltham, MA, USA) supplemented with 5% FBS (Thermo Fisher Scientific, Waltham, MA, USA) and 5% equine serum (Thermo Fisher Scientific, Waltham, MA, USA) and incubated at 37°C and 5% CO_2. For imaging, PC12 cells were plated in 8 well plates (Cellvis, Mountain View, CA, USA) treated with poly-L-lysine (Sigma Aldrich, St. Louis, MO, USA). Cells were transfected with Lipofectamine 2000 (Thermo Fisher Scientific, Waltham, MA, USA) and plasmids (25–100 ng/well) for fluorescently tagged proteins. The EGFP-PLD1 plasmid was a gift from Jeremy Baskin (Bumpus and Baskin, 2017). The PLD1 plasmid is a full-length version of PLD1 with an N-terminal EGFP tag. Specifically, GFP-PLD1 plasmid was made using the PLD1 ORF clone (NCBI accession # BC068976), amplifying it and inserting it into the GFP-C1 vector (Bumpus and Baskin, 2017). VAMP2-pHmScarlet was a gift from Pingyong Xu (Addgene plasmid # 166890). GFP-PASS was a gift from Guangwei Du (Addgene plasmid # 193970). Cells are tested for mycoplasma using the MycoFluor Mycoplasma Detection Kit (Thermo Fisher Scientific, Waltham, MA, USA).

To stimulate fusion, a stimulation buffer containing 3 mM NaCl, 140 mM KCl, 1 mM $MgCl_2$, 3 mM $CaCl_2$, 10 mM D-glucose, and 10 mM HEPES, pH 7.4 (Thermo Fisher Scientific, Waltham, MA, USA) was added to a final concentration (KCl) of 60 mM. In inhibitory experiments, cells were incubated with 0.013% DMSO with or without 100 nM pan-PLD inhibitor 5-fluoro-2-indolyl des-chlorohalopemide (PLD1/2i, Sigma Aldrich, St. Louis, MO, USA) or 500 nM PLD1-specific inhibitor VU0155069 (PLD1i, Sigma Aldrich, St. Louis, MO, USA) for 30 min at 37°C and then imaged immediately. Knockdown experiments were transfected with 8 pmol siRNA (Scramble: AM4635, PLD1: 4390824, Thermo Fisher Scientific, Waltham, MA, USA) and 0.4 μl Lipofectamine 2000 per well for 72 h prior to imaging.

Total internal reflection fluorescence microscopy

PC12 cells were imaged in Fluobrite DMEM (Thermo Fisher Scientific, Waltham, MA, USA) using a TIRF microscope (Nikon Ti-U) equipped with 491 nm and 561 nm lasers, as described previously (Mahmood *et al.*, 2023). A 60 × 1.49 NA objective, a 2.5x magnifying lens, and an EMCCD (Andor iXon897, Abingdon, UK) were used in combination with a DualView (Optical Insights, Suwanee, GA, USA) to split the red and green fluorescence channels onto the camera via a 565LP dichroic with 525/50 and 605/75 emission filters (Chroma Technologies, Bellows Falls, VT, USA). Both color channels were taken simultaneously, and images were collected by MicroManager at 0.109 μm/pixel and 136 ms/frame (Edelstein *et al.*, 2010). For tracking and inhibition studies, cells were imaged on a stage heater at 37°C. Otherwise temperature is noted in the figure captions for all data.

Image analysis

Image analysis was conducted using MATLAB (v. R2021b, Natick, MA, USA) To measure the colocalization of static images, red fluorescent objects in the Syx1a and granule marker images were located using a freely available spot finding routine (Crocker and Grier, 1996). All granules and Syx1a clusters found in the red channel were cropped in the corresponding green channel, making this an objective, object-based analysis, where the user does not choose what is colocalized and what is not. From the cropped green channel images, the, ΔF/S was calculated as follows: $\frac{\Delta F}{S} = \frac{C - A}{A - bg}$, where C is the intensity of a 7 pixel circle in the green channel at a spot found in the red channel, A is a 1-pixel wide concentric ring with one pixel gap from the circle, and bg is the average intensity of the background surrounding the cell.

For measurements that take place in time, movies were corrected for photobleaching by a home-built code to correct to a constant cell intensity. Visiting, docking, and fusing vesicles were found using a previously established algorithm (Mahmood *et al.*, 2023). Here, a difference movie was calculated, max projected, bandpass filtered, and a peak finding algorithm identify spots where a rapid increase of intensity occurs. Locations of intensity changes in the red channel were identified and cropped from the photobleach corrected movies (both green and red). From these cropped movies, intensity plots, calculated as $\frac{\Delta F}{F} = \frac{C_t - C_i}{C_{max} - C_i}$, where C is the intensity of a 7-pixel circle as described in Figure 1 at frame t (C_t) or the frame with the brightest intensity (C_{max}), and C_i is the average initial intensity of a circle for 5 frames prior to onset of intensity increase. From the traces, data is manually binned into visiting, docking, and fusing vesicles. If the trace is not clear, the cropped movie is viewed to determine the fate of the vesicle. Fusion is verified in the movie by an

outward expansion of fluorescence postfusion. For average images of events, only events with at least 50 frames prior to event onset and 100 frames after were included. The bar graphs relating the ΔF/F for PLD1 or PASS intensity were measured at the time corresponding to the peak in intensity for each event for fusion and visiting vesicles. For the docking events, 80% to the plateau of the VAMP2 intensity was used instead of the peak intensity. To determine the relative rate of fusion upon treatment with siRNA, fusion events were identified as described above and counted in cells stimulated with 60 mM KCl, then divided by the average rate of fusion in control cells taken on the same day and from the same cell preparation. All movies were included, even if no fusion events were observed.

To determine the relative PASS intensity for the different stages of fusion the PASS intensity within a circular region divided by the average cell intensity was measured. This corrects for GFP-PASS protein expression levels. To obtain the relative PASS intensity for the visiting (orange), docking (pink), and fusion (blue), the $PASS_{initial}$ intensity for visiting vesicles was subtracted. The formation or accumulation of PA (via PASS intensity) at fusion, docking, and visiting sites is noted by an increase above 0 in the relative intensity and is compared with the $PASS_{initial}$ intensity prior to vesicles visiting.

To determine the mobility of vesicles, tracking of secretory vesicles was done on VAMP2-pHmScarlet vesicles following a previously published analysis (Crocker and Grier, 1996). A position list of peaks was created for each frame, then a tracking algorithm determines tracks from those points. After tracking, the intensity (ΔF/S) of the PLD or PA in the vesicle's position was measured in time using home-built code. The MATLAB code to locate and crop fusion, visiting, and docking events is available on GitHub (https://github.com/michelle-knowles/membrane-fusion) and previously published (Mahmood *et al.*, 2023). JACoP in ImageJ was used to identify the percentage of Syx clusters or secretory vesicles that colocalized with PLD1 using the object-based methods (Bolte and Cordeliéres, 2006).

All statistical significance testing and plotting were conducted using appropriate tests in GraphPad Prism (v. 9.5.1, San Diego, CA, USA) according to published guidelines (Pollard *et al.*, 2019). *P* values were calculated by ANOVA followed by Tukey–Kramer post-hoc test when multiple comparisons were made (Figures 3, A and C, 4G, 5D, and 6D), ANOVA followed by Dunnett's post-hoc test when multiple comparisons were made to one control (Figure 1, D and E), or Student's t-tests when only two things were compared (Figures 2, G and I and 6C). Paired Student's t-tests were used when comparing the same data before and after an event like visiting, fusion, or docking (Figure 6D).

DATA AVAILABILITY

Data generated in this work will be made available from the corresponding author upon reasonable request.

CODE AVAILABILITY

Code for automatic detection of docking, fusion and visiting vesicles has been previously published (Mahmood *et al.*, 2023) and is available on Github (https://github.com/michelleknowles/membrane-fusion). Any other code in this work will be made available from the corresponding author upon reasonable request.

ACKNOWLEDGMENTS

B.L.B. acquired and analyzed data, contributed to writing and experimental design. M.L.H. contributed to data analysis and data acquisition, M.K.K. obtained funds, contributed to writing and data analysis. The work was funded by the National Science Foundation, Chemistry of Life Processes Grant # 1807455.

REFERENCES

Barg, S, Knowles, MK, Chen, X, Midorikawa, M, Almers, W (2010). Syntaxin clusters assemble reversibly at sites of secretory granules in live cells. Proc Natl Acad Sci 107, 20804–20809.

Béglé A, Tryoen-Tóth P, de Barry J, Bader M-F, Vitale N (2009). ARF6 regulates the synthesis of fusogenic lipids for calcium-regulated exocytosis in neuroendocrine cells. J Biol Chem 284, 4836–4845.

Bills BL, Knowles MK (2022). Phosphatidic acid accumulates at areas of curvature in tubulated lipid bilayers and liposomes. Biomolecules 12, 1707.

Bolte S, Cordeliéres FP (2006). A guided tour into subcellular colocalization analysis in light microscopy. J Microsc 224, 213–232.

Brito de Souza L, Pinto da Silva LL, Jamur MC, Oliver C (2014). Phospholipase D is involved in the formation of Golgi associated clathrin coated vesicles in human parotid duct cells. PLoS One 9, e91868.

Brown FD, Thompson N, Saqib KM, Clark JM, Powner D, Thompson NT, Solari R, Wakelam MJO (1998). Phospholipase D1 localises to secretory granules and lysosomes and is plasma-membrane translocated on cellular stimulation. Curr Biol 8, 835–838.

Bumpus TW, Baskin JM (2017). Clickable substrate mimics enable imaging of phospholipase D activity. ACS Cent Sci 3, 1070–1077.

Callan-Jones A, Sorre B, Bassereau P (2011). Curvature-driven lipid sorting in biomembranes. Cold Spring Harb Perspect Biol 3.

Carmon O, Laguerre F, Riachy L, Delestre-Delacour C, Wang Q, Tanguy E, Jeandel L, Cartier D, Thahouly T, Haeberlé A, *et al.* (2020). Chromogranin A preferential interaction with Golgi phosphatidic acid induces membrane deformation and contributes to secretory granule biogenesis. FASEB J 34, 6769–6790.

Caumont A-S, Galas M-C, Vitale N, Aunis D, Bader M-F (1998). Regulated exocytosis in chromaffin cells. J Biol Chem 273, 1373–1379.

Caumont A-S, Vitale N, Gensse M, Galas M-C, Casanova JE, Bader M-F (2000). Identification of a plasma membrane-associated guanine nucleotide exchange factor for ARF6 in chromaffin cells. J Biol Chem 275, 15637–15644.

Chernomordik LV, Kozlov MM (2005). Membrane hemifusion: crossing a chasm in two leaps. Cell 123, 375–382.

Choi WS, Kim YM, Combs C, Frohman MA, Beaven MA (2002). Phospholipases D1 and D2 regulate different phases of exocytosis in mast cells. J Immunol 168, 5682–5689.

Cockcroft S, Way G, O'Luanaigh N, Pardo R, Sarri E, Fensome A (2002). Signalling role for ARF and phospholipase D in mast cell exocytosis stimulated by crosslinking of the high affinity FcεR1 receptor. Mol Immunol 38, 1277–1282.

Corrotte M, Chasserot-Golaz S, Huang P, Du G, Ktistakis NT, Frohman MA, Vitale N, Bader M-F, Grant NJ (2006). Dynamics and function of phospholipase D and phosphatidic acid during phagocytosis. Traffic 7(3):365–77.

Crocker JC, Grier DG (1996). Methods of digital video microscopy for colloidal studies. J Colloid Interface Sci 179, 298–310.

Disse J, Vitale N, Bader M-F, Gerke V (2009). Phospholipase D1 is specifically required for regulated secretion of von Willebrand factor from endothelial cells. Blood 113, 973–980.

Edelstein A, Amodaj N, Hoover K, Vale R, Stuurman N (2010). Computer control of microscopes using μManager. Curr Protoc Mol Biol 92.

Freyberg Z, Sweeney D, Siddhanta A, Bourgoin S, Frohman M, Shields D (2001). Intracellular localization of phospholipase D1 in mammalian cells. Mol Biol Cell 12, 943–955.

Frohman MA (2015). The phospholipase D superfamily as therapeutic targets. Trends Pharmacol Sci 36, 137–144.

Galas M-C, Helms JB, Vitale N, Thiersé D, Aunis D, Bader M-F (1997). Regulated exocytosis in chromaffin cells. J Biol Chem 272, 2788–2793.

Gasman S, Vitale N (2017). Lipid remodelling in neuroendocrine secretion. Biol Cell 109, 381–390.

Haslam R, Coorssen J (1993). Evidence that activation of phospholipase D can mediate secretion from permeabilized platelets. Adv Exp Med Biol 344, 149–164.

Honigmann A, van den Bogaart G, Iraheta E, Risselada HJ, Milovanovic D, Mueller V, Müllar S, Diederichsen U, Fasshauer D, Grubmüller H, *et al.* (2013). Phosphatidylinositol 4,5-bisphosphate clusters act as molecular beacons for vesicle recruitment. Nat Struct Mol Biol 20, 679–686.

Hozumi Y, Yamazaki M, Nakano T (2022). Immunocytochemistry of phospholipase D1 and D2 in cultured cells. Biochem Biophys Res Commun 625, 161–166.

Huang P, Altshuller YM, Hou JC, Pessin JE, Frohman MA (2005). Insulin-stimulated plasma membrane fusion of Glut4 glucose transporter-containing vesicles is regulated by phospholipase D1. Mol Biol Cell 16, 2614–2623.

Hughes WE, Elgundi Z, Huang P, Frohman MA, Biden TJ (2004). Phospholipase D1 regulates secretagogue-stimulated insulin release in pancreatic β-cells. J Biol Chem 279, 27534–27541.
Humeau Y, Vitale N, Chasserot-Golaz S, Dupont J-L, Du G, Frohman MA, Bader M-F, Poulain B (2001). A role for phospholipase D1 in neurotransmitter release. Proc Natl Acad Sci USA 98, 15300.
Jenkins GM, Frohman MA (2005). Phospholipase D: a lipid centric review. Cell Mol Life Sci 62, 2305–2316.
Kassas N, Tanguy E, Thahouly T, Fouillen L, Heintz D, Chasserot-Golaz S, Bader M-F, Grant NJ, Vitale N (2017). Comparative characterization of phosphatidic acid sensors and their localization during frustrated phagocytosis. J Biol Chem 292, 4266–4279.
Knowles MK, Barg S, Wan L, Midorikawa M, Chen X, Almers W (2010). Single secretory granules of live cells recruit syntaxin-1 and synaptosomal associated protein 25 (SNAP-25) in large copy numbers. Proc Natl Acad Sci 107, 20810–20815.
Kooijman EE, Chupin V, Fuller NL, Kozlov MM, de Kruijff B, Burger KNJ, Rand PR (2005). Spontaneous curvature of phosphatidic acid and lysophosphatidic acid. Biochemistry 44, 2097–2102.
Kooijman EE, Chupin V, de Kruijff B, Burger KNJ (2003). Modulation of membrane curvature by phosphatidic acid and lysophosphatidic acid. Traffic 4, 162–174.
Lam AD, Tryoen-Toth P, Tsai B, Vitale N, Stuenkel EL (2008). SNARE-catalyzed fusion events are regulated by Syntaxin1A-lipid interactions. Mol Biol Cell 19, 485–497.
Lang T, Bruns D, Wenzel D, Riedel D, Holroyd P, Thiele C, Jahn R (2001). SNAREs are concentrated in cholesterol-dependent clusters that define docking and fusion sites for exocytosis. EMBO J 20, 2202–2213.
Liu A, Huang X, He W, Xue F, Yang Y, Liu J, Chen L, Yuan L, Xu P (2021). pHmScarlet is a pH-sensitive red fluorescent protein to monitor exocytosis docking and fusion steps. Nat Commun 12, 1413.
Liu L, Liao H, Castle A, Zhang J, Casanova J, Szabo G, Castle D (2005). SCAMP2 interacts with Arf6 and phospholipase D1 and links their function to exocytotic fusion pore formation in PC12 cells. Mol Biol Cell 16, 4463–4472.
Luo L-D, Li G, Wang Y (2017). PLD1 promotes dendritic spine development by inhibiting ADAM10-mediated N-cadherin cleavage. Sci Rep 7, 6035.
Mahmood A, Otruba Z, Weisgerber AW, Palay MD, Nguyen MT, Bills BL, Knowles MK (2023). Exosome secretion kinetics are controlled by temperature. Biophys J 122, 1301–1314.
Matsukawa J, Nakayama K, Nagao T, Ichijo H, Urushidani T (2003). Role of ADP-ribosylation factor 6 (ARF6) in Gastric Acid Secretion. J Biol Chem 278, 36470–36475.
McMahon HT, Kozlov MM, Martens S (2010). Membrane curvature in synaptic vesicle fusion and beyond. Cell 140, 601–605.
Mohrmann R, de Wit H, Verhage M, Neher E, Sørensen JB (2010). Fast vesicle fusion in living cells requires at least three SNARE complexes. Science (1979) 330, 502–505.
Omar-Hmeadi M, Guček A, Barg S (2023). Local PI(4,5)P2 signaling inhibits fusion pore expansion during exocytosis. Cell Rep 42, 112036.
Pelletán LE, Suhaiman L, Vaquer CC, Bustos MA, De Blas GA, Vitale N, Mayorga LS, Belmonte SA (2015). ADP ribosylation factor 6 (ARF6) promotes acrosomal exocytosis by modulating lipid turnover and Rab3A activation. J Biol Chem 290, 9823–9841.
Peng X, Frohman MA (2012). Mammalian phospholipase D physiological and pathological roles. Acta Physiologica 204, 219–226.
Pollard DA, Pollard TD, Pollard KS (2019). Empowering statistical methods for cellular and molecular biologists. Mol Biol Cell 30, 1359–1368.
Rohrbough J, Broadie K (2005). Lipid regulation of the synaptic vesicle cycle. Nat Rev Neurosci 6, 139–150.
Stepien KP, Rizo J (2021). Synaptotagmin-1–, Munc18-1–, and Munc13-1–dependent liposome fusion with a few neuronal SNAREs. Proc Natl Acad Sci 118, e2019314118.
Stutchfield J, Cockcroft S (1993). Correlation between secretion and phospholipase D activation in differentiated HL60 cells. Biochem J 293, 649–655.
Tanguy E, Costé de Bagneaux P, Kassas N, Ammar M-R, Wang Q, Haeberlé A-M, Raherindratsara J, Fouillen L, Renard P-Y, Montero-Hadjadje M, *et al*. (2020). Mono- and poly-unsaturated phosphatidic acid regulate distinct steps of regulated exocytosis in neuroendocrine cells. Cell Rep 32, 108026.
Tanguy E, Wolf A, Wang Q, Chasserot-Golaz S, Ory S, Gasman S, Vitale N (2022). Phospholipase D1-generated phosphatidic acid modulates secretory granule trafficking from biogenesis to compensatory endocytosis in neuroendocrine cells. Adv Biol Regul 83, 100844.
Vitale N, Caumont A-S, Chasserot-Golaz S, Du G, Wu S, Sciorra VA, Morris AJ, Frohman MA, Bader M-F (2001). Phospholipase D1: a key factor for the exocytotic machinery in neuroendocrine cells. EMBO J 20, 2424–2434.
Vitale N, Chasserot-Golaz S, Bader M-F (2002a). Regulated secretion in chromaffin cells. Ann N Y Acad Sci 971, 193–200.
Vitale N, Chasserot-Golaz S, Bailly Y, Morinaga N, Frohman MA, Bader M-F (2002b). Calcium-regulated exocytosis of dense-core vesicles requires the activation of ADP-ribosylation factor (ARF)6 by ARF nucleotide binding site opener at the plasma membrane. J Cell Biol 159, 79–89.
Wang Q, Wolf A, Ozkan S, Richert L, Mely Y, Chasserot-Golaz S, Ory S, Gasman S, Vitale N (2023). V-ATPase modulates exocytosis in neuroendocrine cells through the activation of the ARNO-Arf6-PLD pathway and the synthesis of phosphatidic acid. Front Mol Biosci 10, 1163545.
Weber T, Zemelman BV, McNew JA, Westermann B, Gmachl M, Parlati F, Söllner TH, Rothman JE (1998). SNAREpins: minimal machinery for membrane fusion. Cell 92, 759–772.
Yang CZ, Mueckler M (1999). ADP-ribosylation factor 6 (ARF6) defines two insulin-regulated secretory pathways in adipocytes. J Biol Chem 274, 25297–25300.
Zeniou-Meyer M, Zabari N, Ashery U, Chasserot-Golaz S, Haeberlé A-M, Demais V, Bailly Y, Gottfried I, Nakanishi H, Neiman AM, *et al*. (2007). Phospholipase D1 production of phosphatidic acid at the plasma membrane promotes exocytosis of large dense-core granules at a late stage. J Biol Chem 282, 21746–21757.
Zeniou-Meyer M, Béglé A, Bader M-F, Vitale N (2009). The Coffin-Lowry syndrome-associated protein RSK2 controls neuroendocrine secretion through the regulation of phospholipase D1 at the exocytotic sites. Ann NY Acad Sci 1152, 201–208.
Zhang F, Wang Z, Lu M, Yonekubo Y, Lian X, Zhang Y, Wu P, Zhou Y, Grinstein S, Hancock JF, Du G (2014). Temporal production of the signaling lipid phosphatidic acid by phospholipase D2 determines the output of extracellular signal-regulated kinase signaling in cancer cells. Mol Cell Biol 34, 84–95.